longfin causes *cis*-ectopic expression of the *kcnh2a ether-a-go-go* K^+ channel to autonomously prolong fin outgrowth

Scott Stewart[1*], Heather K. Le Bleu[1, 2], Gabriel A. Yette[1, 2], Astra L. Henner[1], Joshua A. Braunstein[1], Kryn Stankunas[1, 2*]

[1]Institute of Molecular Biology
[2]Department of Biology
University of Oregon
297A Klamath Hall
1370 Franklin Blvd
Eugene, OR 97403-1229
Office: (541) 346-7416
Fax: (541) 346-4854

* Correspondence: sstewar2@uoregon.edu; kryn@uoregon.edu

ABSTRACT

Organs stop growing to achieve the size and shape characteristic of the species and in scale with the animal's body. Likewise, regenerating organs sense injury extents to instruct appropriate replacement growth. Fish fins exemplify both phenomena through their tremendous diversity of form and remarkably robust regeneration. The classic zebrafish mutant *longfin* develops and regenerates dramatically elongated fins and underlying bony ray skeleton. We recently showed *longfin* disrupts the orderly depletion of a growth-promoting blastema "niche" sub-population during fin regeneration. Initial niche sizes correlate with the amount of niche-generating intra-ray mesenchyme released from variably sized and tapered rays upon injury. Therefore, skeletal geometry-defined positional information and niche depletion dynamics can explain robust fin size restoration. Here, we find the *longfin* eponymous phenotype is entirely caused by *cis* over-expression of *kcnh2a*, a voltage-gated potassium channel related to human *ether-a-go-go*. Temporal delivery of a small molecule inhibitor confirms Kcnh2a actively extends the fin outgrowth period. We use blastula transplantations to show *longfin*-expressed *kcnh2a* acts tissue autonomously in the intra-ray mesenchyme/niche lineage, where it is concordantly ectopically expressed. We propose membrane potential dynamics and downstream ion signaling promote niche-to-mesenchyme transitions to progressively slow outgrowth and thereby establish and restore fin size and shape.

MAIN TEXT

60 The shapes and sizes of fish fins are remarkably diverse to optimize swimming, predator avoidance, and courtship while contributing to fishes' aesthetic appeal (Nelson et al., 2016). Zebrafish illustrate how fins develop with stereotypical shapes and then grow in scale with the rest of the animal. Remarkably, amputated adult fins regenerate to their original size and shape regardless of the degree of injury (reviewed in Chen and Poss, 2017).

65 Zebrafish fin geometries are defined by underlying skeletons comprised of segmented and cylindrical bony rays surrounded by a stratified epidermis. Each ray segment represents two opposing hemi-cylindrical bones produced by tightly associated osteoblasts. Vasculature, sensory axons and mesenchymal cells reside within the rays. Rays extend developmentally and during regeneration by sequential addition of bone segments at the distal end of the growing fin 70 (Goldsmith et al., 2003; Iovine and Johnson, 2000). Adult fin regenerative outgrowth likely recapitulates developmental mechanisms and, with their larger size and rapid regeneration, is the focus of fin size control studies.

After injury, fin regeneration initiates by de-differentiation of mature cells to lineage-restricted progenitors forming a regeneration-specific anatomical structure termed a blastema 75 (Knopf et al., 2011; Singh et al., 2012; Sousa et al., 2011; Stewart and Stankunas, 2012; Tu and Johnson, 2011). The heterogeneous blastema organizes by cell lineage and state to enable progressive regeneration (reviewed in Wehner and Weidinger, 2015). De-differentiated osteoblasts that lose hallmarks of mature bone cells to become proliferative progenitor osteoblasts (pObs) migrate to blastema peripheries. pObs also hierarchically arrange along the 80 distal-to-proximal axis of the blastema, with the most progenitor "state" cells distally concentrated (Stewart et al., 2014). Similarly, mesenchymal cells residing between hemi-rays de-

differentiate, form the major blastema population radially interior to pObs, and then contribute to regenerated intra-ray tissue (Tornini et al., 2016). Some intra-ray mesenchymal cells transition into specialized distal blastema cells, termed an "orchestrating center", that produce growth factors including Wnt signals sustaining progenitor osteoblasts (Stewart et al., 2014; Wehner et al., 2014). As presented in the accompanying manuscript, we refer to this population as a "niche" to reflect its role generating a growth-favoring environment including by sustaining surrounding cells in progenitor states (Morrison and Spradling, 2008; Stewart et al., 2019). A small quiescent sub-group of niche cells reside at the extreme distal blastema (Nechiporuk and Keating, 2002; Tornini et al., 2016). However, the niche itself includes proliferating cells and, like pObs, is maintained by Wnt signals (Nechiporuk and Keating, 2002; Stewart et al., 2019; Wehner et al., 2014).

Niche cells first appear in the distal blastema about two days after amputation. The niche pool then gradually declines over the course of regeneration, in part from re-differentiation to intra-ray mesenchyme (Stewart et al., 2019). A correlation between niche size and growth rate and the niche's growth-promoting properties suggests that niche-to-mesenchymal cell state transitions ensure correct extent of fin growth. We extended this observation with mathematical modeling to propose skeletal geometry of variably sized and tapered bony rays provides de facto "positional information" by setting the amount of niche generated upon injury (Stewart et al., 2019). By this "transpositional scaling" model, the progressive depletion of the niche, and therefore its ability to support pObs, inherently restores overall fin size and shape as well as tapered ray geometries. Regardless of this model's ultimate resilience, understanding reversible niche-mesenchyme cell state transitions would reveal fin outgrowth control mechanisms.

Analysis of fin growth in zebrafish mutants provides insight into mechanisms of
105 appendage scaling (Van Eeden et al., 1996). One classic example, the dominant *longfin*^{t2} (*lof*^{t2}) allele, develops and regenerates exceptionally long fins (Elias, 1984; Van Eeden et al., 1996), resulting in a "schleierform", or flowing veil-like appearance (Fig. 1A and B). Notably, the widely used stock strain *Tüpfel-Longfin* (*TL*) contains compound *lof*$^{t2/t2}$*; leopard*$^{t1/t1}$ mutations, whose respective fin and pigmentation phenotypes allow visual identification of mixed
110 genotypes (Haffter et al., 1996).

Fins of *lof*^{t2} fish do not grow faster (Iovine and Johnson, 2000; Stewart et al., 2019). Rather, *lof*^{t2} fins fail to stop growing, characterized by the iterative addition of new ray segments (Iovine and Johnson, 2000). Correspondingly, we demonstrated mesenchyme-derived niche cells fail to deplete over time in fin-regenerating *lof*^{t2} fish (Stewart et al., 2019). As such, the *lof*^{t2}
115 mutant provides a genetic entry point to discover mechanisms of niche cell depletion and therefore size control during fin growth and regeneration. Further motivated by the historical significance and prominence of *lof*^{t2} in the zebrafish field, we sought to identify the cause of its eponymous phenotype.

The dominant phenotype of *lof*^{t2}, mapped to a ~250 kilobase region of chromosome 2
120 (chr2), is suppressed by deletion of a region encompassing the locus (Iovine and Johnson, 2002). Therefore, *lof*^{t2} likely results from a dominant negative or gain-of-function mutation rather than haploinsufficiency. One explanation is that *lof*^{t2} alters a transcriptional regulatory element causing over- or ectopic expression of a gene(s) within or near the *lof* region (Fig. 1C). To test this, we used mRNA sequencing (RNA-seq) to identify differentially expressed genes (DEGs).
125 We compared transcriptomes of *lof*$^{t2/+}$ and wildtype clutchmate caudal fins 4 days post amputation (dpa) since this immediately precedes the onset of differential growth. We used

dissected distal fin regenerates (Fig. 1D) given *lof*^{t2} disrupts behavior of distal-residing niche cells (Stewart et al., 2019). Across the genome, we identified 39 increased and 111 decreased DEGs (+/- 2-fold change) (Table S1). Confining the DEG analysis to the *lof*^{t2} region and
130 surrounding genes (Fig. 1C), a single transcript roughly 1 megabase from *lof*^{t2}, *potassium voltage-gated channel, subfamily H (eag-related), member 2a* (*kcnh2a*), was overexpressed in *lof*$^{t2/+}$ animals (+ 25.8 fold) (Fig. 1D). Quantitative RT-PCR (RT-qPCR) confirmed *kcnh2a* was expressed specifically in *lof*$^{t2/+}$ fins (Fig. 1D inset).

To determine if *lof*^{t2} affects *kcnh2a* expression in *cis* or *trans*, we leveraged sequence
135 polymorphisms (Butler et al., 2015) in the 5' UTR that distinguish *kcnh2a* from *TL* and *WIK* (*kcnh2a*$^{WIK\text{-}TL}$) strains versus our wildtype *AB* fish stocks (*kcnh2a*^{AB}) (Fig. 1E). We used allele-specific primers and RT-qPCR to observe that *kcnh2a*$^{WIK\text{-}TL}$ transcripts accounted for nearly all *kcnh2a* expression in *lof*^{t2} *kcnh2a*$^{WIK\text{-}TL}$; *lof*$^{+}$ *kcnh2a*^{AB} regenerating caudal fins (Fig. 1E). The apparent 10% residual contribution of *kcnh2a*^{AB} to total *kcnh2a* expression likely reflects primer
140 cross-hybridization or weak *trans* effects of *lof*^{t2}. We conclude that most, if not all, *kcnh2a* expression in *lof*^{t2} regenerating fins arises from *cis* effects of the *lof*^{t2} mutation.

To determine if overexpressed *kcnh2a* causes *lof*^{t2} fin overgrowth, we used CRISPR/Cas9 to mutate *kcnh2a* in the *TL* (*leo*$^{t1/t1}$; *lof*$^{t2/t2}$) background. We outcrossed founders to wildtype fish and identified numerous obligatory *lof*$^{t2/+}$ F_1 animals with normal sized fins carrying germline-
145 transmitted *kcnh2a* loss-of-function alleles. One of these, *kcnh2a*^{b1391}, contained an 8 bp deletion causing a frameshift at codon 3 of the predicted polypeptide. Homozygous *lof*$^{t2/t2}$; *kcnh2a*$^{b1391/b1391}$ fish were phenotypically normal with fin sizes indistinguishable from wildtype clutchmates (Fig. 2A and B). Caudal fin regeneration of *lof*$^{t2/t2}$; *kcnh2a*$^{b1391/b1391}$ and wildtype animals also was identical (Fig. S1). Since *lof*^{t2} *kcnh2a*^{b1391}; *lof*$^{+}$ *kcnh2a*$^{+}$ and *lof*^{t2} *kcnh2a*^{b1391};

150 *lof*^{t2} *kcnh2a*$^{+}$ fish developed normal and long fins, respectively, the *kcnh2a*^{b1391} allele likely suppresses *lof*^{t2} in *cis*. Finally, *lof*^{t2}-linked *kcnh2a* had no exon or intron/exon boundary non-synonymous mutations or unappreciated SNPs. We conclude that *cis*-ectopic expression of *kcnh2a* on the *lof*^{t2} chr2 causes the *lof*^{t2} fin overgrowth phenotype. Therefore, *lof*^{t2} is a neomorphic and regulatory mutant allele of *kcnh2a*.

155 Kcnh2a is related to *ether-a-go-go* voltage-gated K^{+} channels (Vandenberg et al., 2012). Inhibition of its closest human orthologue KCNH2 (hERG) is responsible for the off-target effects of a number of now discontinued drugs. For example, the once-favored anti-histamine astemizole causes serious cardiac arrhythmias by directly inhibiting KCNH2 (Sanguinetti and Tristani-Firouzi, 2006; Suessbrich et al., 1996; Zhou et al., 1999). The onset of appreciable fin 160 overgrowth in regenerating *lof*^{t2} fins occurs around 7 dpa (Stewart et al., 2019). Therefore, we treated *lof*$^{t2/+}$ fish with astemizole from 7-30 dpa to determine if Kcnh2a is actively required for fin overgrowth. This astemizole regimen perfectly suppressed excessive *lof*$^{t2/+}$ fin outgrowth to wildtype levels ($p < 0.005$; Fig. 2C-F). Therefore, Kcnh2a causes fin overgrowth by preventing growth termination and, consistent with normal fin development and regeneration in 165 *kcnh2a*$^{b1391/b1391}$ fish, Kcnh2a is not involved in normal fin growth.

Kcnh2a could function fin autonomously or systemically (e.g., via circulating endocrine factors) to promote overgrowth in *lof*^{t2}. A straightforward prediction of the tissue autonomous model is fin ray size heterogeneity in *lof*$^{t2/+}$ fish with mosaic *kcnh2a* loss-of-function mutations. In contrast, the systemic hypothesis predicts that deleterious mutations of *kcnh2a* on *lof*^{t2} chr2 170 concomitantly would suppress overgrowth of all fins. We used F_0 CRISPR/Cas9 targeting to induce mosaic mutations at the *kcnh2a* locus and discriminate between these scenarios. We carried out this experiment in *lof*$^{t2/+}$ rather than *lof*$^{t2/t2}$ fish to sensitize suppression of fin

overgrowth. We observed partial fin growth suppression in 25% (17 of 68) of *kcnh2a* CRISPR-targeted F_0 fish reared to adulthood (Fig. 3A, B). One striking example displayed one rescued
175 pectoral fin of wildtype length with the other exhibiting pronounced overgrowth indicative of *lof*^{t2} (Fig. 3B). We genotyped both pectoral fins at the *kcnh2a* CRISPR targeting site and readily detected insertions/deletions (indels) in the phenotypically suppressed fin (Fig. 3B). We conclude *kcnh2a* likely functions in fin tissue to produce overgrown fins.

We next explored whether specific cell lineages harboring *lof*^{t2}, and therefore potentially
180 ectopic Kcnh2a, are sufficient for fin overgrowth. We generated chimeras by blastula cell transplantations (Kimmel et al., 1990), introducing EGFP-labeled *lof*$^{t2/+}$ blastula-stage cells into *AB* wildtype host embryos and raising them to adulthood. Roughly 13% of transplants (39 fins with overgrowth from 28 of 214 screened chimeras) exhibited EGFP$^+$ fin tissue with notable overgrowth indicative of chimerism (Fig. 3C and Fig. S2). Several fins had EGFP$^+$ overgrown
185 rays flanked by intermediate length rays lacking robust EGFP expression. We attribute this to diffusible factors emanating from the primary overgrown ray, anatomical influences on growth between adjacent rays, or scarce EGFP$^+$ cells sufficient to cause lesser overgrowth. In a few cases, chimeric animals displayed asymmetrically-sized pectoral fins, as observed with *kcnh2a* CRISPR-targeted F_0 *lof*^{t2} mosaic fish (Fig. S2). All overgrown chimeric rays contained EGFP$^+$
190 intra-ray mesenchymal cells, although EGFP-expressing osteoblasts and epidermis also were evident in some cases (Fig. 3C). We immunostained fin sections with Msx antibodies marking intra-ray mesenchyme (Stewart et al., 2019) to confirm this lineage, the source of niche cells, always included EGFP$^+$ *lof*$^{t2/+}$-derived cells in overgrown chimeric fins (Fig. 3D and Fig. S2). In contrast, chimeras harboring only EGFP$^+$ *lof*$^{t2/+}$ epidermal cells were of normal length (Fig. S3).
195 As *lof*^{t2} intra-ray mesenchyme is sufficient for fin overgrowth, Kcnh2a likely acts in these cells

and/or their derivative niche cells to slow niche-to-mesenchyme transitions and thereby prolong outgrowth.

We used RNAscope (Wang et al., 2012) to determine the expression pattern of *kcnh2a* mRNA in 4 dpa *TL* caudal fin sections. *kcnh2a* was expressed robustly in *TL* proximal intra-ray
200 cells with relatively lower levels in blastema mesenchyme and presumptive distal niche cells (Fig. 4A). In contrast, we did not detect *kcnh2a* in *AB* control fins, as expected from RNA-Seq and qRT-PCR (Fig. 4B). We next combined *kcnh2a* RNAscope with immunostaining for the Msx or *tph1b:mCherry* (Tornini et al., 2016) intra-ray mesenchyme lineage markers. *kcnh2a* was expressed in Msx^{+} or *tph1b:mCherry*$^{+}$ cells in proximal regenerating tissue (Fig. 4C-F) with
205 lower levels in distal *tph1b:mCherry*$^{+}$ presumptive niche cells (Fig. S4). While levels vary, *lof*^{t2}-driven specific and ectopic *kcnh2a* expression in intra-ray mesenchyme and niche cells of regenerating fins (Fig. 4C-F) reinforces Kcnh2a acts in this lineage to promote fin overgrowth.

Originally isolated by tropical fish hobbyists, *lof*^{t2} was one of the first zebrafish mutant lines used scientifically (hence, its "t2" – Tübingen 2 – designation) (Elias, 1984; Haffter et al.,
210 1996; Van Eeden et al., 1996). *lof*^{t2} remains widely used, with its fin overgrowth a convenient phenotypic marker to discriminate zebrafish of mixed genotypes. By demonstrating Kcnh2a causes *lof*^{t2}, we help resolve the origins of its remarkable and long appreciated phenotype. We show the *lof*^{t2} mutation causes *cis*-ectopic expression of a *kcnh2a,* an apparent long distance regulatory effect, although a chromosomal re-arrangement linking *kcnh2a* to a displaced
215 enhancer is also possible. At present, the precise *lof*^{t2} genetic lesion remains unknown. Likewise, we have not explored if *kcnh2a* is misexpressed in other *lof*^{t2} tissues where it could adversely affect excitable cell behaviors. If so, *lof*^{t2} likely should be avoided as a "wildtype" strain.

Human KCNH2 produces I_{Kr}, the rapid component of the cardiac delayed rectifier current (Curran et al., 1995; Noble and Tsien, 1969; Sanguinetti et al., 1995). *KCNH2* mutations are a
220 frequent cause of inherited arrythmias known as long QT syndrome whereby patients exhibit prolonged cardiac action potentials (Bohnen et al., 2017; Curran et al., 1995; Sanguinetti et al., 1995). The voltage-dependent gating properties of KCNH2, namely slow opening and closing but fast inactivation, uniquely enables it to repolarize cardiac tissue and terminate action potentials (Bohnen et al., 2017; Vandenberg et al., 2012). Presumably sharing these
225 electrophysiological properties, the ability of Kcnh2a voltage-gated channel activity to disrupt intra-ray mesenchyme lineage suggests their behaviors normally are regulated by dynamic changes in membrane potential.

The accompanying manuscript presents a mathematical model exploring how niche cell dynamics impact regenerative fin growth (Stewart et al., 2019). We modeled the extent of
230 outgrowth in terms of three "scaling parameters": β, which determines how many niche cells initially are generated as a function of ray capacity to harbor mesenchyme, k_l, which defines the potency of niche cells to promote outgrowth, and α, which sets the net rate of niche depletion (Stewart et al., 2019). By varying these parameters and comparing theoretical to actual growth rates, we attributed fin overgrowth in *lof*^{t2} to an increase in α indicative of slower depletion of
235 growth-sustaining niche cells. Accordingly, we observed niche cell perdurance in regenerating *lof*^{t2} fins (Stewart et al., 2019). Therefore, identifying Kcnh2a as the cause of fin overgrowth in *lof*^{t2} links its K^+ channel activity to niche-to-mesenchyme state transitions, likely by altered membrane repolarization kinetics and accompanying inopportune activation of other voltage-gated ion channels. Disrupted downstream ion signaling may directly (within niche cells) or

240 indirectly (within mesenchyme to produce secreted negative feedback signals acting on niche cells) promote niche cells to return to a mesenchymal state.

Bioelectricity is extensively linked to organ size control and regeneration (McLaughlin and Levin, 2018), including by additional zebrafish fin overgrowth models disrupting ion channels and ion-dependent signaling. Gain-of-function mutations in the K^+ channel *kcnk5b* in

245 *another longfin* (*alf*) develop and regenerate long fins (Perathoner et al., 2014). Further, fin overgrowth in the *schleier* mutant is caused by loss of *kcc4a/ slc12a7a*, a K^+ Cl^- cotransporter likely expressed in intra-ray mesenchyme (Lanni et al., 2019). A straightforward hypothesis is the mutations in *kcnh2a*, *kcnk5b*, and *kcc4a* converge on a common target to promote fin overgrowth. A strong candidate effector is the Ca^{2+}-dependent phosphatase calcineurin, whose

250 acute inhibition causes dramatic fin overgrowth (Kujawski et al., 2014). Ca^{2+} dynamics are strongly influenced by ion channel activity and KCNH2 negatively modulates Ca^{2+} signaling during the cardiac conduction cycle (Roden et al., 2002). Moreover, epistasis studies indicate *kcnk5b* and calcineurin cooperate to regulate fin growth (Daane et al., 2018). However, unlike *lof*^{t2}, overgrown fins in these other models display additional abnormalities including fewer ray

255 segments and tissue hyper-vascularization (Kujawski et al., 2014; Lanni et al., 2019; McMillan et al., 2018; Perathoner et al., 2014). These pleiotropic phenotypes suggest independent, multi-lineage defects or that overgrowth can originate from correctly numbered but individually longer ray segments due to inhibited joint formation. The latter seems unlikely since *evx1* mutants lack all ray segment joints and have normal sized fins (Schulte et al., 2011; Ton and Iovine, 2013).

260 Regardless, defining relative niche and mesenchyme states in other ion signaling-linked overgrowth models may further explain how bioelectricity regulates cell state transitions and therefore fin size control.

Our study identifying ectopic *kcnh2a* as the cause of the classic *lof*^{t2} zebrafish allele provides a framework to consider bioelectric control of organ size variation and regeneration
265 through ion-mediated intracellular signaling regulation of cell state transitions. Key next steps include characterizing membrane potentials, putative depolarizing signals, and how downstream ion signaling regulates gene expression and behavior of intra-ray mesenchyme and/or niche cells during fin development and regeneration.

270 **MATERIALS AND METHODS**

Zebrafish strains and maintenance

Zebrafish were housed in the University of Oregon Aquatic Animal Care Services facility at 28-29°C. The University of Oregon Institutional Animal Care and Use Committee oversaw animal
275 use. Wildtype *AB* (University of Oregon Aquatic Animal Care Services), *TL* (Haffter et al., 1996), *Tg(tph1b:mCherry)* (Tornini et al., 2016), *Tg(sp7:EGFP)* (DeLaurier et al., 2010), and *Tg(eab:FlEx)* (Boniface et al., 2009) zebrafish lines were used.

Generating *kcnh2a* mutants

280 To mutate *kcnh2a* on the mutant lof^{t2} chromosome 2, a guide RNA encompassing the putative start codon (in bold) 5' GACAAC**ATG**CCTGTACGACG 3' was synthesized in vitro and co-injected with recombinant Cas9 protein (500 ng/μl; Thermo Fisher) into one-cell stage *TL* embryos, and reared to adulthood as described previously (Hwang et al., 2013). These F_0 fish were outcrossed and embryos analyzed by PCR using primers kcnh2a_P1 and kcnh2a_P2 and
285 DNA sequencing to identify mutations. The F1 clutches harboring mutant alleles were then reared to adulthood and adults were genotyped by using primers kcnh2a_P1 and kcnh2a_P2 and DNA sequencing. This resulted in the identification a predicted non-sense allele, $kcnh2a^{b1391}$, that deletes 8 bp (underlined) at the guide RNA target site (GACAAC**ATG**CCTGTACGACG), resulting in a frame-shift at codon 3 of the predicted polypeptide and loss of a Hpy99I restriction
290 endonuclease cleavage site. Genotyping of $kcnh2a^{b1391}$ was carried out by amplifying genomic DNA using primers kcnh2a_P1 and kcnh2a_P2 and digesting the resulting PCR products with Hpy99I.

To detect *kcnh2a* mutations in *TL* fish, exons were PCR amplified using *TL* genomic DNA (primers listed below), ligated to a vector (pCRII, Thermo) and sequenced using T7 and
295 SP6 primers. In some cases, additional sequencing primers were used to ensure complete coverage of the clone.

To distinguish between a tissue autonomous vs. systemic function for *kcnh2a* in promoting fin outgrowth in $lof^{t2/+}$, CRISPR/Cas9 experiments were carried out on one-cell stage embryos from a $lof^{t2/+}$ x $lof^{+/+}$ cross. Animals were raised to adulthood and caudal fins were
300 scored for fin ray size heterogeneity.

Adult whole zebrafish and fin imaging

High resolution fin images were obtained by first euthanizing animals with tricaine and mounting fins in 0.75% low melting agarose. Stitched differential interference contrast (DIC)
305 images were then captured using a Nikon Eclipse Ti widefield microscope with a 10x objective and NIS-Elements software. Whole-animal images were captured using a homemade light box made from a fenestrated styrofoam container, a halogen bicycle lamp, and a consumer Fujifilm X-A1 camera with Fujinon 28mm 1.4R lens.

310 **RNA-Seq**

Caudal fins of adult $lof^{t2/+}$ and $lof^{+/+}$ *Tg(sp7:EGFP)* (DeLaurier et al., 2010) clutchmates were amputated. At 4 dpa, regenerated tissue beyond the GFP-marked differentiated osteoblast domain was homogenized in TRIzol reagent (Thermo Fisher). Tissue pooled from four animals constituted matched replicate samples. RNA was isolated following the manufacturer's
315 instructions with minor alterations. The RNA was precipitated overnight at -80°C and then

pelleted at 15,000 rpm for 30 minutes at 4°C. Pellets were washed twice with 70% ethanol, dried for 10 minutes at room temperature, and resuspended in RNase-free water (Thermo Fisher).

RNA-Seq libraries were prepared from 1 μg of isolated RNA using a Kapa Biosystems Stranded mRNA-Seq kit. Bar-coded libraries were pooled and sequenced using a HiSeq 4000 (Illumina) and reads were aligned to the zebrafish genome (GRCz11) using TopHat2 (Kim et al., 2013). Aligned reads were scored using HTseq (Anders et al., 2015) and edgeR (Robinson et al., 2010) was used to identify differentially expressed transcripts (-/+ 2.0 fold).

RT-qPCR

To confirm overexpression of *kcnh2a* in *lof*^{t2} animals, RNA was isolated from whole caudal fin regenerates of adult *lof*$^{t2/+}$ and *lof*$^{+/+}$ clutchmates at 96 hpa. Each replicate represented a pooled sample of three fin regenerates. RNA was isolated as previously described. cDNA was synthesized from 500 ng of total RNA using Maxima H Minus RT (Thermo Fisher) and the manufacturer's protocol. Oligo(dT)18 was used to prime reverse transcription. Primers *kcnh2a*_P1 and *kcnh2a*_P2 were used to determine in *kcnh2a* expression. Primers for *runx2a* and *rpl13* (Stewart et al., 2014) were used as a control and ubiquitously expressed reference gene, respectively.

The *kcnh2a*^{AB} polymorphism (Fig. 1E) was identified serendipitously in University of Oregon Aquatic Animal Care Services facility stock AB fish during the course of these studies and was identified by PCR amplification using primers *kcnh2a*_P1 + *kcnh2a*_P2, followed by Sanger sequencing. The *kcnh2a*^{AB} polymorphism was present in a number of stock facility AB fish and has been observed previously in other zebrafish strains (Butler et al., 2015).

To demonstrate monoallelic expression of *kcnh2a* on mutant *lof*^{t2} chromosome 2, we generated *lof*^{t2} *kcnh2a*$^{WIK\text{-}TL}$*; lof*$^{+}$ *kcnh2a*^{AB} fish and prepared cDNA from 4 dpa caudal fins as
340 described above. Quantitative PCR was carried out using this cDNA as template and the following primer combinations: *kcnh2a*_P1 and *kcnh2a*_P2, *kcnh2a*_P1 and *kcnh2a*$^{WIK\text{-}TL}$, and *kcnh2a*_P1 and *kcnh2a*^{AB}. For all studies, qPCR was quantified by the $\Delta\Delta C_t$ method using *rpl13* mRNA levels for normalization as described (Stewart et al., 2014). The statistical analysis used a repeated measures one-way ANOVA with Tukey's multiple comparisons test. Transcript levels
345 from the non-*lof*^{t2} chromosome *kcnh2a*^{AB} allele were significantly lower than both total *kcnh2a* and *kcnh2a*$^{WIK\text{-}TL}$ produced from the *lof*^{t2} chromosome (both $p < 0.0001$).

Small molecule treatments

Fins of *lof*$^{t2/+}$ and clutchmate animals were amputated and allowed to regenerate for 7 days. At 7
350 dpa, astemizole (5mM in DMSO) was added directly to fish water to a final concentration of 500 nM; control fish received an equal volume of DMSO. Fish were fed and changed to fresh drug- or DMSO-containing water every 48 hours. At 30 dpa, each animal's caudal fin was imaged on a Leica M205 FA stereomicroscope and lengths of the third ray from the amputation site to the fin's tip were measured (detailed below). For each experimental group, a representative animal
355 was selected and imaged by DIC and stitched imaging as described above.

Fin measurements

To quantify fin growth after regeneration, the length of the third ray was measured from the amputation site to the end of the fin from images acquired with a Leica M205 FA
360 stereomicroscope. Growth measurements from individuals comprising each cohort were

averaged and normalized the control group. A one-way ANOVA with Tukey's multiple comparisons tests tested differences between regenerated fin lengths for the *kcnh2a* loss-of-function genetic rescue experiment ($p < 0.0001$ between *lof*$^{t2/t2}$ and either wildtype or *lof*$^{t2/t2}$; *kcnh2a*$^{b1391/b1391}$ fish; no difference between wildtype and *lof*$^{t2/t2}$; *kcnh2a*$^{b1391/b1391}$ genotypes. A
365 two-way ANOVA with Bonferroni's multiple comparisons test assessed statistical significance for the astemizole fin regeneration rescue experiment ($p < 0.0001$ DMSO-treated from 7-30 dpa comparing wildtype and *lof*$^{t2/+}$ fin lengths, no significant differences between genotypes at 7 dpa or comparing 7-30 dpa astemizole-treated wildtype and *lof*$^{t2/+}$ regenerative outgrowth).

370 **Immunostaining**

To carry out antibody staining on sections, tissue was paraffin embedded and sectioned essentially as described earlier (Stewart et al., 2014). Slides were subjected to antigen retrieval for 5 minutes in a pressure cooker in a solution of 1 mM EDTA, 0.1% Tween-20, followed by blocking in 10% milk in phosphate buffered saline containing 0.1% Tween-20. Antibodies were
375 applied overnight in blocking solution at 4°C. Individual antigens were visualized using Alexa dye-conjugated secondary antibodies (Thermo Fisher). Imaging of antibody stained sections was carried out on Olympus FV1000 or Zeiss LSM880 laser scanning confocal microscopes.

RNAscope and immunostaining

380 RNAscope probes to detect *kcnh2a* mRNA were designed and synthesized by ACD Bio. RNAscope was performed using the Multiplex Fluorescent kit (ACD Bio) according to manufacturer's recommendations on paraffin embedded fin sections with minor modifications. Immunostaining using Msx (Developmental Studies Hybridoma Bank; 1:20 dilution of

hybridoma culture supernatant) or mCherry (Sicgen; 1:100) antibodies was carried out after
385 RNAscope as directed by the manufacturer (ACD Bio). Nuclei were visualized by Hoechst staining (Thermo Fischer). Imaging used Olympus FV1000 or Zeiss LSM880 laser scanning confocal microscopes.

Generation of chimeric animals

390 Blastula-stage cell transplantations were performed as described (Kimmel et al., 1990). Briefly, 20-50 single cells from high-stage *lof*$^{t2/+}$*; Tg(eab:FlEx)* donors were transplanted into *AB* host high-stage embryos (Kimmel et al., 1995). Chimeric animals were reared to adulthood and fins screened for EGFP expression and overgrowth. Those with apparent fin overgrowth were imaged on a Leica M205 FA stereomicroscope. Stitched high resolution images of select overgrown fins
395 were also collected. Epifluorescent images of overgrown fins were analyzed to determine lineages EGFP^{+} cells, essentially as described in (Stewart and Stankunas, 2012). Lineages of select samples were confirmed by immunostaining representative examples using EGFP (Aves Labs Inc.; 1:1000), Msx (DSHB; 1:20, sp7 A-13 (Santa Cruz Biotechnology; 20 ng/ml) and p63 PA5-36069 (Thermo; 1:100) antibodies as outlined below.

400

Primers

The following primers were employed in this study:

kcnh2a_P1	5’ GGATTTGCGCCCTCCGAACACTAAC 3’
kcnh2a_P2	5’ GTGCGCGCATCCTCGAGCTCAG 3’
405 kcnh2a_P3	5’ ACTGGAGACTTTGAAGAGACGC 3’
kcnh2a_P4	5’ GAATGATGGTGTCCAGAAAGGT 3’

snai2_P1	5’ ACGACAAGACAGGACCATTTTT 3’
snai2_P2	5’ TGCAGTTAAAATGACCAAATCC 3’
kcnh2a^{AB}	5’ GTACAGGCATGTTTGTCCC 3’
kcnh2a^{WIK-TL}	5’ GTACAGGCATGTTGTCCT 3’
kcnh2a_exon_1-2_for	5’ CCCCAACCATCCTCTCACTGCCTCTCC 3’
kcnh2a_exon_1-2_rev	5’ CAGGGCCCCTAAGCTGTCCTGG 3’
kcnh2a_exon_3_for	5’ CTGGTGATCGCAGACCTTAACACAGACCTC 3’
kcnh2a_exon_3_rev	5’ GAATTGACCCCCTCCCTGATCGTCAACG 3’
kcnh2a_exon_4_for	5’ CTGGTGAACTGCTGCAAGTAAGTTACTGTAGATTC 3’
kcnh2a_exon_4_rev	5’ CTGTATGACCACTGTATGACCAGGTGTACC 3’
kcnh2a_exon_5_for	5’ GTACAGAGGTGGTGGTCCTCCAGGAACGTGG 3’
kcnh2a_exon_5_rev	5’ GTCTGTGGTGAATACACCATGTGTGCCTTTTAAAT 3’
kcnh2a_exon_6_for	5’ CAGCAGCATTTACTTCAATCACGATGATCAC 3’
kcnh2a_exon_6_rev	5’ GGTTTGGAGCCACCTGAGTGTGAG 3’
kcnh2a_exon_7_for	5’ GCACCCTAGCAACTGTAATAACTGCTGC 3’
kcnh2a_exon_7_rev	5’ GAATAAGCACTTAGCAGCACTAACCTCCG 3’
kcnh2a_exon_8-9_for	5’ GTTCAACCACTGGGTGTCAAACTTACACACT 3’
kcnh2a_exon_8-9_rev	5’ GGGTGGGGAGTGTCTGGGTAAGGG 3’
kcnh2a_exon_10-12_for	5’ GGCATGCAGCGCCACCTGCTGTTGATTTC 3’
kcnh2a_exon_10-12_rev	5’ GGTACGGCAACTATTCTCCCAATCAACATAC 3’
kcnh2a_exon_13-14_for	5’ GAGGTTAGAATGACTTGAATGAGTATAATCAGTG 3’
kcnh2a_exon_13-14_rev	5’ GACCCAGCCGAGGCTTGAACCA 3’
kcnh2a_exon_15_for	5’ GAGGGTGTGTGATATCAATAGCATGGGG 3’

430	kcnh2a_exon_15_rev	5’ GCGTTCACACAGCACAGCGTAACCAG 3’

ACKNOWLEDGEMENTS

We thank the University of Oregon Aquatic Animal Care Services for animal husbandry, A. Lasseigne and A. Miller for assisting with blastula transplantations, J. Chehab for sequence analysis, the Stankunas lab for discussions, C. Kimmel, D. Grimes, and V. Lewis for manuscript feedback, and K. Poss for providing the *Tg(tph1b:mCherry)* line.

FOOTNOTES

Competing interests

None.

Author contributions

S. S., H. K. L., G. A. Y., and K. S. designed experiments. S. S., H. K. L., G. A. Y., A. L. H., and J. A. B. performed experiments. S. S. and K. S. prepared and wrote the manuscript with input from H. K. L., G. A. Y., and A. L. H.

Funding

The National Institutes of Health (NIH) provided research funding (1R01GM127761 (K. S. and S. S.) and 5R03AR067522 (S. S.)). G. A. Y. was supported by a NIH NRSA graduate fellowship (5F31AR071283). H. K. L. received support from the University of Oregon NIH-funded Developmental Biology Training Program (5T32HD007348).

Data and material availability

RNA-Seq data are deposited at the NCBI Gene Expression Omnibus GSE137352. Requests for materials should be addressed to S. S. and K. S.

REFERENCES

455 **Anders, S., Pyl, P. T. and Huber, W.** (2015). HTSeq--a Python framework to work with high-throughput sequencing data. *Bioinformatics* **31**, 166–169.

Bohnen, M. S., Peng, G., Robey, S. H., Terrenoire, C., Iyer, V., Sampson, K. J. and Kass, R. S. (2017). Molecular Pathophysiology of Congenital Long QT Syndrome. *Physiol. Rev.* **97**, 89–134.

460 **Boniface, E. J., Lu, J., Vicotroff, T., Zhu, M. and Chen, W.** (2009). FlEx-based transgenic reporter lines for visualization of Cre and Flp activity in live zebrafish. *Genesis (New York, N.Y. : 2000)* **47**, 484–491.

Butler, M. G., Iben, J. R., Marsden, K. C., Epstein, J. A., Granato, M. and Weinstein, B. M. (2015). SNPfisher: tools for probing genetic variation in laboratory-reared zebrafish.
465 *Development* **142**, 1542–1552.

Chen, C.-H. and Poss, K. D. (2017). Regeneration Genetics. *Annu. Rev. Genet.* **51**, 63–82.

Curran, M. E., Splawski, I., Timothy, K. W., Vincent, G. M., Green, E. D. and Keating, M. T. (1995). A molecular basis for cardiac arrhythmia: HERG mutations cause long QT syndrome. *Cell* **80**, 795–803.

470 **Daane, J. M., Lanni, J., Rothenberg, I., Seebohm, G., Higdon, C. W., Johnson, S. L. and Harris, M. P.** (2018). Bioelectric-calcineurin signaling module regulates allometric growth and size of the zebrafish fin. *Sci Rep* **8**, 10391.

DeLaurier, A., Eames, B. F., Blanco Sánchez, B., Peng, G., He, X., Swartz, M. E., Ullmann, B., Westerfield, M. and Kimmel, C. B. (2010). Zebrafish sp7:EGFP: A transgenic for
475 studying otic vesicle formation, skeletogenesis, and bone regeneration. *Genesis* **48**, 505–511.

Elias, J. (1984). *Brachydanio frankei*-Schleierform. *Aquaria* **34**, 81–85.

Goldsmith, M. I., Fisher, S., Waterman, R. and Johnson, S. L. (2003). Saltatory control of isometric growth in the zebrafish caudal fin is disrupted in long fin and rapunzel mutants. *Developmental Biology* **259**, 303–317.

480 **Haffter, P., Odenthal, J., Mullins, M. C., Lin, S., Farrell, M. J., Vogelsang, E., Haas, F., Brand, M., Van Eeden, F. J., Furutani-Seiki, M., et al.** (1996). Mutations affecting pigmentation and shape of the adult zebrafish. *Dev. Genes Evol.* **206**, 260–276.

Hwang, W. Y., Fu, Y., Reyon, D., Maeder, M. L., Tsai, S. Q., Sander, J. D., Peterson, R. T., Yeh, J.-R. J. and Joung, J. K. (2013). Efficient genome editing in zebrafish using a
485 CRISPR-Cas system. *Nat. Biotechnol.* **31**, 227–229.

Iovine, M. K. and Johnson, S. L. (2000). Genetic analysis of isometric growth control mechanisms in the zebrafish caudal Fin. *Genetics* **155**, 1321–1329.

Iovine, M. K. and Johnson, S. L. (2002). A genetic, deletion, physical, and human homology map of the long fin region on zebrafish linkage group 2. *Genomics* **79**, 756–759.

Kim, D., Pertea, G., Trapnell, C., Pimentel, H., Kelley, R. and Salzberg, S. L. (2013). TopHat2: accurate alignment of transcriptomes in the presence of insertions, deletions and gene fusions. *Genome Biol.* **14**, R36.

Kimmel, C. B., Ballard, W. W., Kimmel, S. R., Ullmann, B. and Schilling, T. F. (1995). Stages of embryonic development of the zebrafish. *Dev. Dyn.* **203**, 253–310.

Kimmel, C. B., Warga, R. M. and Schilling, T. F. (1990). Origin and organization of the zebrafish fate map. *Development* **108**, 581–594.

Knopf, F., Hammond, C., Chekuru, A., Kurth, T., Hans, S., Weber, C. W., Mahatma, G., Fisher, S., Brand, M., Schulte-Merker, S., et al. (2011). Bone Regenerates via Dedifferentiation of Osteoblasts in the Zebrafish Fin. *Developmental Cell* **20**, 713–724.

Kujawski, S., Lin, W., Kitte, F., Börmel, M., Fuchs, S., Arulmozhivarman, G., Vogt, S., Theil, D., Zhang, Y. and Antos, C. L. (2014). Calcineurin regulates coordinated outgrowth of zebrafish regenerating fins. *Developmental Cell* **28**, 573–587.

Lanni, J. S., Peal, D., Ekstrom, L., Chen, H., Stanclift, C., Bowen, M. E., Mercado, A., Gamba, G., Kahle, K. T. and Harris, M. P. (2019). Integrated K+ channel and K+Cl- cotransporter function are required for the coordination of size and proportion during development. *Developmental Biology*.

McLaughlin, K. A. and Levin, M. (2018). Bioelectric signaling in regeneration: Mechanisms of ionic controls of growth and form. *Developmental Biology* **433**, 177–189.

McMillan, S. C., Zhang, J., Phan, H.-E., Jeradi, S., Probst, L., Hammerschmidt, M. and Akimenko, M.-A. (2018). A regulatory pathway involving retinoic acid and calcineurin demarcates and maintains joint cells and osteoblasts in regenerating fin. *Development* **145**, dev161158.

Morrison, S. J. and Spradling, A. C. (2008). Stem cells and niches: mechanisms that promote stem cell maintenance throughout life. *Cell* **132**, 598–611.

Nechiporuk, A. and Keating, M. T. (2002). A proliferation gradient between proximal and msxb-expressing distal blastema directs zebrafish fin regeneration. *Development* **129**, 2607–2617.

Nelson, J. S., Grande, T. C. and Wilson, M. (2016). *Fishes of the World*. Fifth Edition. John Wiley & Sons.

Noble, D. and Tsien, R. W. (1969). Outward membrane currents activated in the plateau range of potentials in cardiac Purkinje fibres. *J. Physiol. (Lond.)* **200**, 205–231.

Perathoner, S., Daane, J. M., Henrion, U., Seebohm, G., Higdon, C. W., Johnson, S. L., Nüsslein-Volhard, C. and Harris, M. P. (2014). Bioelectric signaling regulates size in zebrafish fins. *PLoS Genet* **10**, e1004080.

Robinson, M. D., McCarthy, D. J. and Smyth, G. K. (2010). edgeR: a Bioconductor package for differential expression analysis of digital gene expression data. *Bioinformatics* **26**, 139–140.

Roden, D. M., Balser, J. R., George, A. L. and Anderson, M. E. (2002). Cardiac ion channels. *Annu. Rev. Physiol.* **64**, 431–475.

Sanguinetti, M. C. and Tristani-Firouzi, M. (2006). hERG potassium channels and cardiac arrhythmia. *Nature* **440**, 463–469.

Sanguinetti, M. C., Jiang, C., Curran, M. E. and Keating, M. T. (1995). A mechanistic link between an inherited and an acquired cardiac arrhythmia: HERG encodes the IKr potassium channel. *Cell* **81**, 299–307.

Schulte, C. J., Allen, C., England, S. J., Juárez-Morales, J. L. and Lewis, K. E. (2011). Evx1 is required for joint formation in zebrafish fin dermoskeleton. *Dev. Dyn.* **240**, 1240–1248.

Singh, S. P., Holdway, J. E. and Poss, K. D. (2012). Regeneration of amputated zebrafish fin rays from de novo osteoblasts. *Developmental Cell* **22**, 879–886.

Sousa, S., Afonso, N., Bensimon-Brito, A., Fonseca, M., Simões, M., Leon, J., Roehl, H., Cancela, M. L. and Jacinto, A. (2011). Differentiated skeletal cells contribute to blastema formation during zebrafish fin regeneration. *Development* **138**, 3897–3905.

Stewart, S. and Stankunas, K. (2012). Limited dedifferentiation provides replacement tissue during zebrafish fin regeneration. *Developmental Biology* **365**, 339–349.

Stewart, S., Gomez, A. W., Armstrong, B. E., Henner, A. and Stankunas, K. (2014). Sequential and opposing activities of Wnt and BMP coordinate zebrafish bone regeneration. *Cell Reports* **6**, 482–498.

Stewart, S., Yette, G. A., Le Bleu, H. K., Henner, A. L., Braunstein, J. A., Chehab, J. W., Harms, M. J. and Stankunas, K. (2019). Skeletal geometry and niche transitions restore organ size and shape during zebrafish fin regeneration. *bioRxiv* 606970.

Suessbrich, H., Waldegger, S., Lang, F. and Busch, A. E. (1996). Blockade of HERG channels expressed in Xenopus oocytes by the histamine receptor antagonists terfenadine and astemizole. *FEBS Lett.* **385**, 77–80.

Ton, Q. V. and Iovine, M. K. (2013). Identification of an evx1-dependent joint-formation pathway during FIN regeneration. *PLOS ONE* **8**, e81240.

555 **Tornini, V. A., Puliafito, A., Slota, L. A., Thompson, J. D., Nachtrab, G., Kaushik, A.-L., Kapsimali, M., Primo, L., Di Talia, S. and Poss, K. D.** (2016). Live Monitoring of Blastemal Cell Contributions during Appendage Regeneration. *Curr. Biol.* **26**, 2981–2991.

Tu, S. and Johnson, S. L. (2011). Fate restriction in the growing and regenerating zebrafish fin. *Developmental Cell* **20**, 725–732.

560 **Van Eeden, F. J., Granato, M., Schach, U., Brand, M., Furutani-Seiki, M., Haffter, P., Hammerschmidt, M., Heisenberg, C. P., Jiang, Y. J., Kane, D. A., et al.** (1996). Genetic analysis of fin formation in the zebrafish, Danio rerio. *Development* **123**, 255–262.

Vandenberg, J. I., Perry, M. D., Perrin, M. J., Mann, S. A., Ke, Y. and Hill, A. P. (2012). hERG K(+) channels: structure, function, and clinical significance. *Physiol. Rev.* **92**, 1393–
565 1478.

Wang, F., Flanagan, J., Su, N., Wang, L.-C., Bui, S., Nielson, A., Wu, X., Vo, H.-T., Ma, X.-J. and Luo, Y. (2012). RNAscope: a novel in situ RNA analysis platform for formalin-fixed, paraffin-embedded tissues. *J Mol Diagn* **14**, 22–29.

Wehner, D. and Weidinger, G. (2015). Signaling networks organizing regenerative growth of
570 the zebrafish fin. *Trends Genet.* **31**, 336–343.

Wehner, D., Cizelsky, W., Vasudevaro, M. D., Özhan, G., Haase, C., Kagermeier-Schenk, B., Röder, A., Dorsky, R. I., Moro, E., Argenton, F., et al. (2014). Wnt/β-catenin signaling defines organizing centers that orchestrate growth and differentiation of the regenerating zebrafish caudal fin. *Cell Reports* **6**, 467–481.

575 **Zhou, Z., Vorperian, V. R., Gong, Q., Zhang, S. and January, C. T.** (1999). Block of HERG potassium channels by the antihistamine astemizole and its metabolites desmethylastemizole and norastemizole. *J. Cardiovasc. Electrophysiol.* **10**, 836–843.

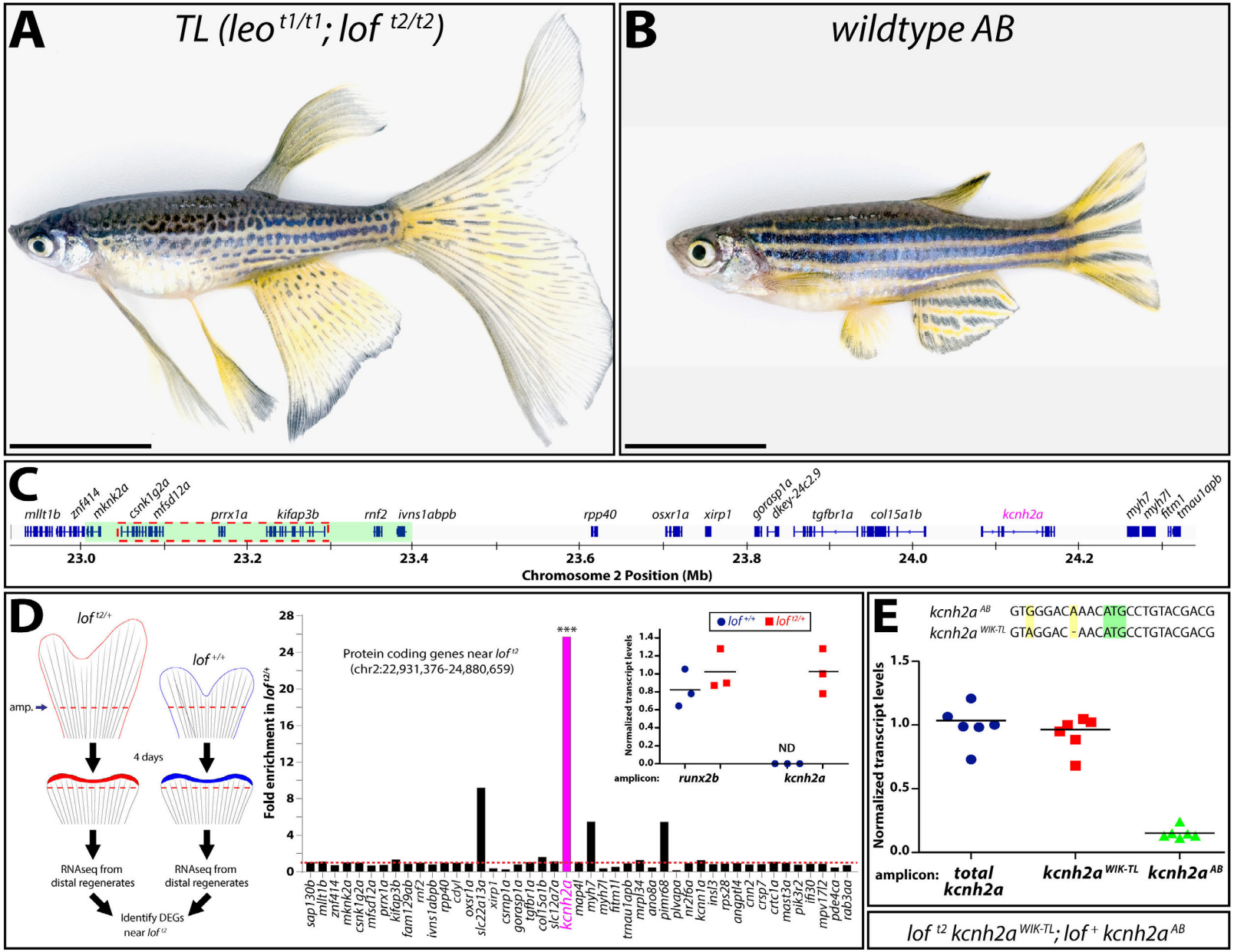
A
TL (leo t1/t1; lof t2/t2)
B
wildtype AB
C
mllt1b znf414 mknk2a csnk1g2a mfsd12a prrx1a kifap3b rnf2 ivns1abpb rpp40 osxr1a xirp1 gorasp1a dkey-24c2.9 tgfbr1a col15a1b kcnh2a myh7 myh7l fitm1 tmau1apb
23.0 23.2 23.4 23.6 23.8 24.0 24.2
Chromosome 2 Position (Mb)
D
lof t2/+
lof +/+
amp.
4 days
RNAseq from distal regenerates
RNAseq from distal regenerates
Identify DEGs near lof t2
Protein coding genes near lof t2
(chr2:22,931,376-24,880,659)
Fold enrichment in lof t2/+
***
sap130b mllt1b znf414 mknk2a csnk1g2a mfsd12a prrx1a kifap3b fam129ab rnf2 ivns1abpb rpp40 cayl oxsr1a slc22a13a xirp1 csrnp1a gorasp1a tgfbr1a col15a1b slc12a7a kcnh2a map4l myh7 myh7l fitm1l tmau1apb mrpl34 ano8a pimr68 plvapa nr2f6a kcnn1a insl3 rps28 angptl4 cnn2 csp7 crtc1a mast3a pik3r2 ifn30 mpv17l2 pde4ca rab3aa
lof +/+ lof t2/+
Normalized transcript levels
ND
amplicon: runx2b kcnh2a
E
kcnh2a AB GTGGGACAAACATGCCTGTACGACG
kcnh2a WIK-TL GTAGGAC - AACATGCCTGTACGACG
Normalized transcript levels
amplicon: total kcnh2a kcnh2a WIK-TL kcnh2a AB
lof t2 kcnh2a WIK-TL; lof + kcnh2a AB

Figure 1

Figure 1. The *lof*^{t2} mutation causes *cis*-ectopic expression of *kcnh2a*. (A, B) Bright-field images of adult *TL(Tüpfel longfin: leo*$^{t1/t1}$*; lof*$^{t2/t2}$*)* and wildtype *AB* zebrafish. The scale bar represents 1 cm. (**C**) Schematic diagram of 1.5 Mb region of zebrafish chromosome 2 (chr2). The putative location of the *lof*^{t2} mutation is outlined with a dashed red line and the region
585 deleted in the suppressed *lof*^{tg1} is highlighted by a green box as determined in (Iovine and Johnson, 2002). **(D) Left.** Schematic of RNA-Seq experimental design to identify genes mis-expressed in *lof*^{t2}. **Right.** RNA-Seq data showing gene expression changes on chr2:22,931,376-24,880,659 from *lof*$^{t2/+}$ relative to clutchmate *lof*$^{+/+}$ controls. The asterisks indicate $p < 10^{-5}$. **Inset.** Expression of *kcnh2a* in *lof*$^{t2/+}$ (in red) and *lof*$^{+/+}$ (in blue) clutchmates determined by RT-
590 qPCR using 4 dpa fin cDNA. Data were normalized to *rpl13* reference expression levels and presented as fold change relative to *lof*$^{t2/+}$. *runx2b* expression levels are shown for comparative purposes and were not significantly changed between the two genotypes. Expression of *kcnh2a* was below limits of detection in *lof*$^{+/+}$ fish (indeterminate, ND). Each point represents a cohort of 3 animals. **(E)** RT-qPCR on 4 dpa caudal fin cDNA from *lof*^{t2} *kcnh2a*$^{WIK\text{-}TL}$*; lof*$^{+}$ *kcnh2a*^{AB} fish to
595 detect chromosome-specific expression *kcnh2a.* Sequences of non-coding *kcnh2a* polymorphisms that specifically amplify either *kcnh2a*$^{WIK\text{-}TL}$, located on the *lof*^{t2} mutant chr2 (red squares), or *kcnh2a*^{AB}, located on *AB* chr2 (green triangles). Data were normalized to total *kcnh2a* (blue ovals) levels determined using primers that amplify either allele indiscriminately. Each data point represents data from an individual fish.

600

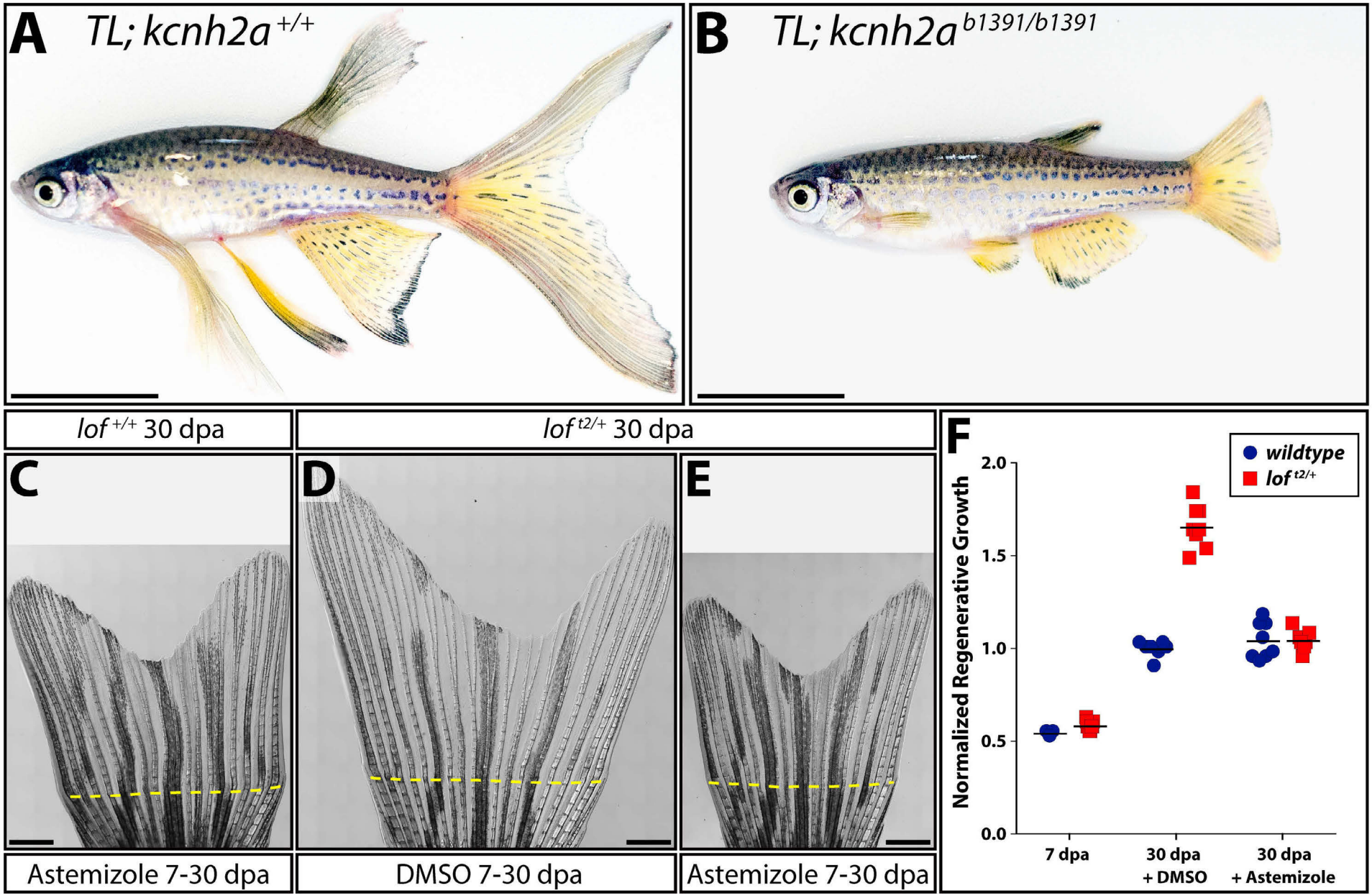
A
TL; kcnh2a +/+
B
TL; kcnh2a b1391/b1391
lof +/+ 30 dpa
lof t2/+ 30 dpa
C
D
E
Astemizole 7-30 dpa
DMSO 7-30 dpa
Astemizole 7-30 dpa
F
wildtype
lof t2/+
Normalized Regenerative Growth
2.0
1.5
1.0
0.5
0.0
7 dpa
30 dpa + DMSO
30 dpa + Astemizole

Figure 2

Figure 2. *lof*^{t2} is caused by gain of Kcnh2a activity during fin outgrowth.

(A, B) Brightfield images of clutchmate *TL; kcnh2a*$^{+/+}$ (panel A) and *TL; kcnh2a*$^{-/-}$ (panel B) adult zebrafish. The scale bars represent 1 cm. **(C-E)** Stitched DIC images showing clutchmate
605 *lof*$^{+/+}$ astemizole-treated (panel C; 500 nM), DMSO-treated *lof*$^{t2/+}$ (panel D) and *lof*$^{t2/+}$, astemizole-treated (panel E; 500 nM) fish at 30 days post caudal fin amputation (dpa). The dashed yellow line indicates the amputation plane and the scale bars denote 1 mm. **(F)** Quantification of normalized caudal fin regenerative outgrowth from control and astemizole-treated animals. Data points represent individual *lof*$^{+/+}$ (red squares) and *lof*$^{t2/+}$ (blue circles)
610 animals prior to treatment (7 dpa) and post-treatment (30 dpa) with DMSO or astemizole (500 nM). Graph shows mean lengths of the third ventral regenerated ray normalized to DMSO-treated controls at 30 dpa. Each point is an individual animal.

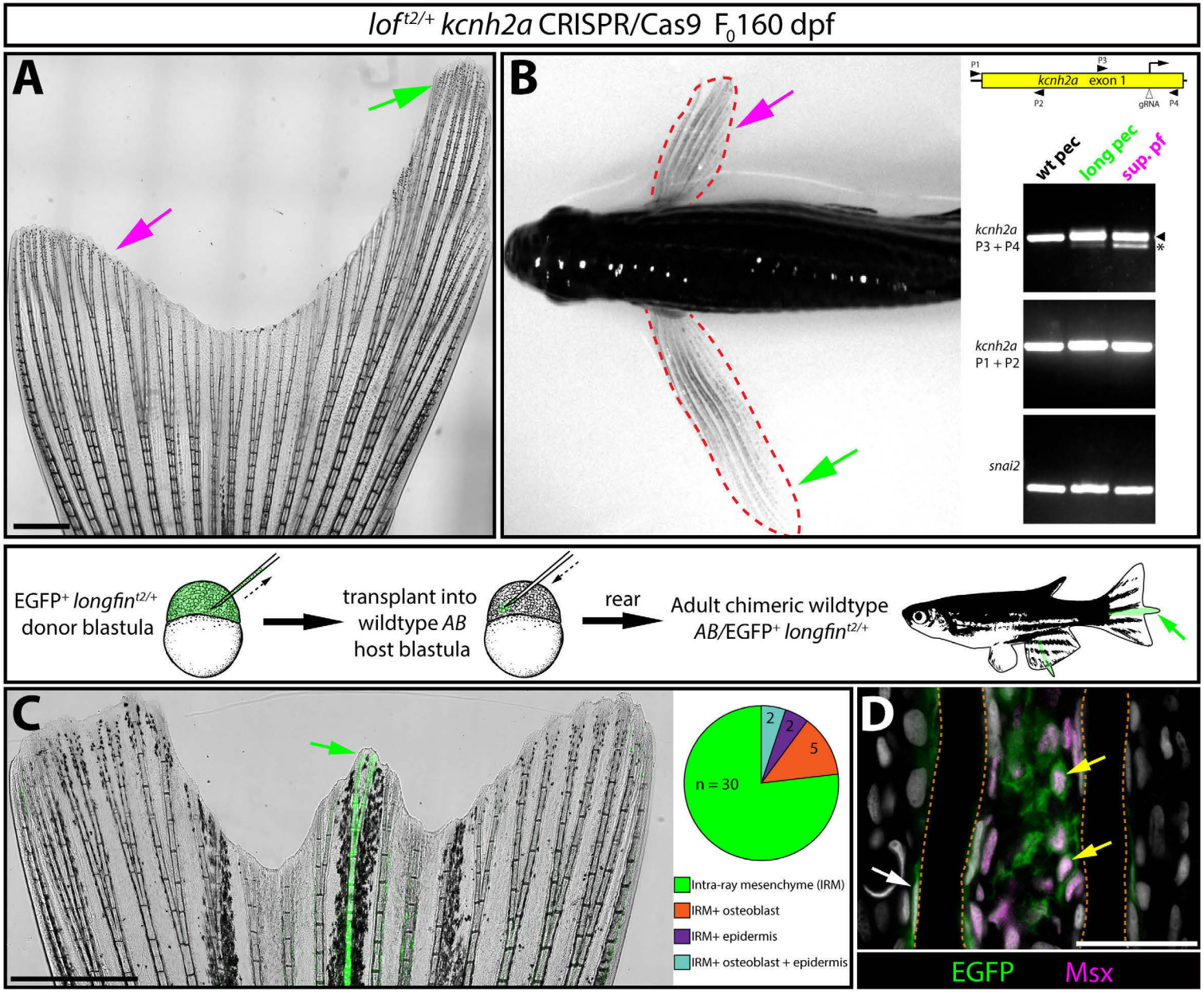
lof t2/+ kcnh2a CRISPR/Cas9 F0 160 dpf
A
B
P1
P3
kcnh2a exon 1
P2
gRNA
P4
wt pec
long pec
sup. pf
kcnh2a P3 + P4
kcnh2a P1 + P2
snai2
EGFP+ longfin t2/+ donor blastula
transplant into wildtype AB host blastula
rear
Adult chimeric wildtype AB/EGFP+ longfin t2/+
C
n = 30
2
2
5
Intra-ray mesenchyme (IRM)
IRM+ osteoblast
IRM+ epidermis
IRM+ osteoblast + epidermis
D
EGFP
Msx

Figure 3

Figure 3. *kcnh2a* acts fin autonomously and within the intra-ray mesenchyme/niche lineage to promote overgrowth.

(A) Representative whole mount image of a *kcnh2a* F_0 CRISPR *lof*$^{t2/+}$ adult caudal fin. The magenta arrow points to suppressed overgrowth in otherwise long fins (green arrow). The scale
620 bar represents 1 mm. **(B)** Pectoral fin asymmetry in a *kcnh2a* F_0 CRISPR *lof*$^{t2/+}$ animal. The magenta arrow points to a wildtype-sized fin indicative of phenotypic suppression. The green arrow points to the expected overgrown contralateral fin. Genomic DNA from these fins was used to amplify regions flanking the *kcnh2a* guide RNA (top panel), upstream of the guide sequence (middle panel), and at an unrelated control locus, *snai2* (bottom panel). The arrowhead
625 shows the expected *kcnh2a* amplicon using primers flanking the guide RNA target; the asterisk points to indels in the fin displaying a suppressed (sup.) *lof*^{t2} phenotype. **(C)** Upper panel schematic highlighting the nature of the blastula stage transplant experiment. EGFP$^+$ *lof*$^{t2/+}$ blastula cells were transplanted into wildtype *AB* embryos. Reared adults with partial or complete fin overgrowth were scored for cell type(s) with EGFP expression. Panel C shows a
630 representative example of a caudal fin displaying overgrown EGFP$^+$ fin rays (green arrow). The green arrows point to overgrown EGFP$^+$ fin rays and the scale bar represents 1 mm. The chart indicates the EGFP$^+$ lineage(s) present in 39 overgrown regions across 30 total fins with extended rays. **(D)** Caudal fin section containing an overgrown chimeric fin ray immunostained with EGFP and Msx antibodies. Yellow arrows point to EGFP$^+$/Msx$^+$ intra-ray mesenchymal
635 cells. The white arrow highlights an EGFP$^+$ osteoblast. Fin rays are outlined with a dashed orange line. Hoechst-stained nuclei are in gray. The scale bar represent 50 μm.

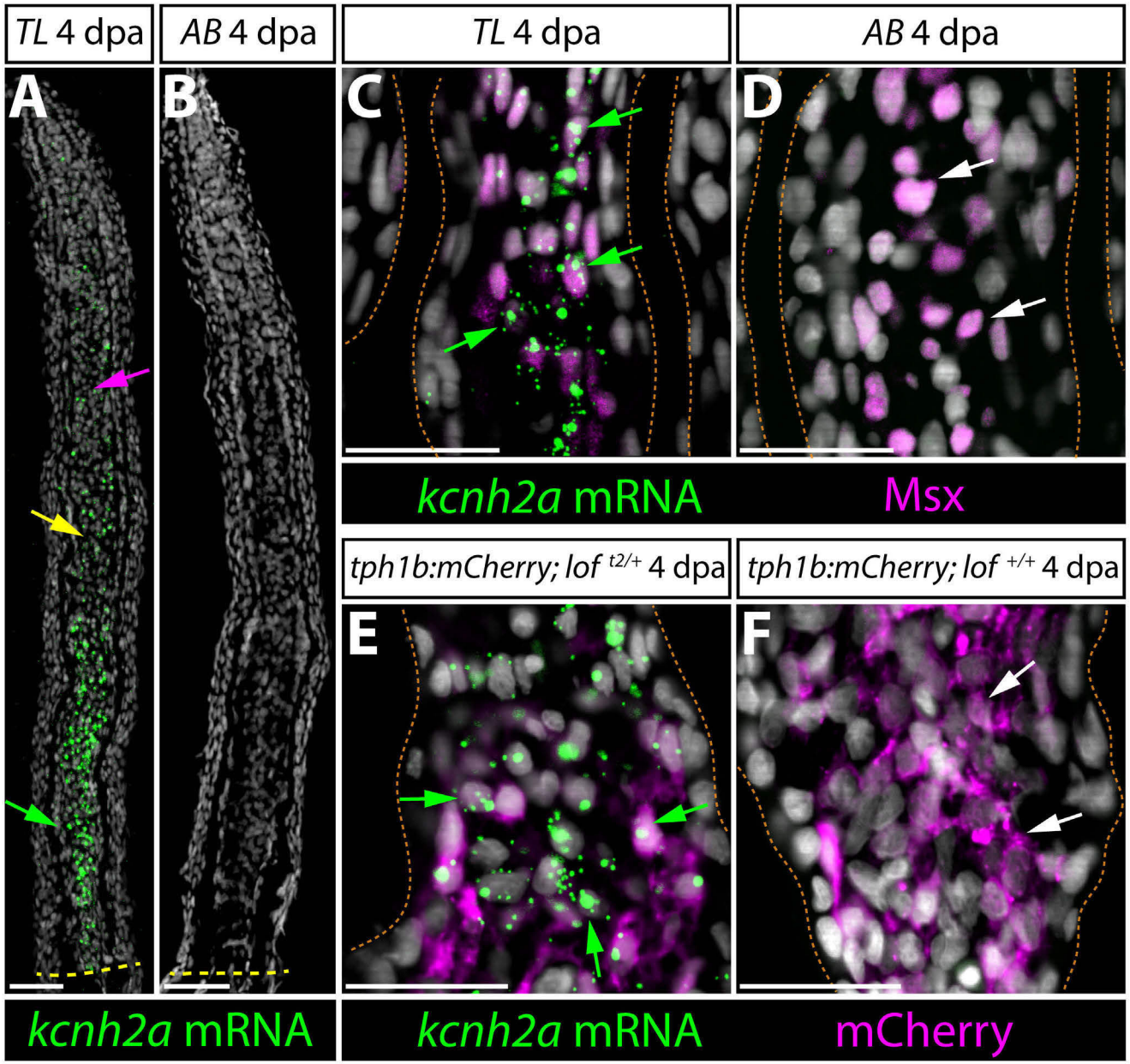
TL 4 dpa
AB 4 dpa
TL 4 dpa
AB 4 dpa
A
B
C
D
kcnh2a mRNA
Msx
tph1b:mCherry; lof t2/+ 4 dpa
tph1b:mCherry; lof +/+ 4 dpa
E
F
kcnh2a mRNA
kcnh2a mRNA
mCherry

Figure 4

Figure 4. *kcnh2a* is expressed ectopically in *lof*^{t2} intra-ray mesenchyme lineage cells during
640 **fin regeneration.**

(A, B) *kcnh2a* mRNA localization (in green) detected by RNAscope in longitudinal caudal fin sections from 4 day post amputation (dpa) *TL* (*lof*$^{t2/t2}$, panel A) and *AB* (panel B) animals. The green arrow points to proximal intra-ray cells expressing high levels of *kcnh2a*, which is also detected in medial mesenchyme (yellow arrow) and distal cells (magenta arrow) of *TL* fish. The
645 dashed yellow line denotes the site of amputation. Hoechst stained nuclei are in gray and scale bars indicate 50 μm. **(C, D)** Double *kcnh2a* RNAscope (green) and Msx immunostaining (magenta) of 4 dpa caudal fin sections from *TL* (panel C) and *AB* (panel D) fish. **(E, F)** Combination *kcnh2a* RNAscope (green) and mCherry immunostaining (magenta) of 4 dpa fin sections from (E) *tph1b:mCherry; lof*$^{t2/+}$ and (F) *tph1b:mCherry; lof*$^{+/+}$ fish. For panels C-F,
650 green arrows highlight Msx^{+} or *tph1b:mCherry*$^{+}$ cells with overlapping *kcnh2a* mRNA in proximal regenerating *lof* tissue. White arrows show Msx^{+} or *tph1b:mCherry*$^{+}$ nuclei in corresponding regions from control fins lacking *kcnh2a* expression. Fin rays are outlined with a dashed orange line. Hoechst stained nuclei are in gray. Scale bars represent 50 μm.

655 **SUPPLEMENTARY INFORMATION**

Figures S1-S4.

Table S1.

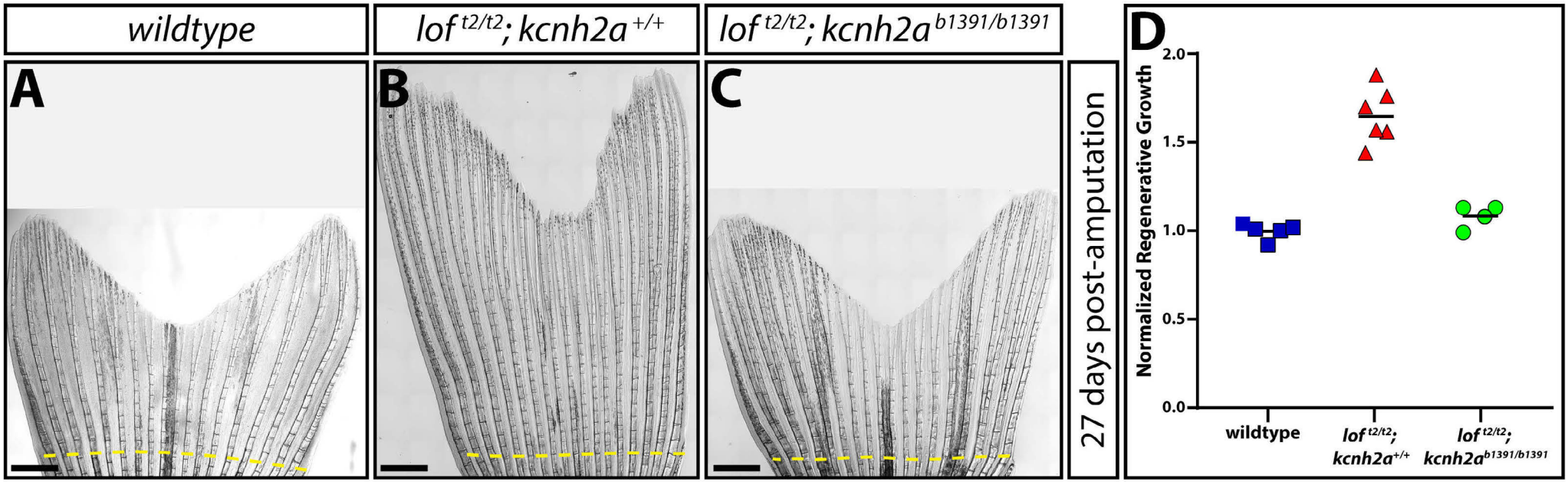

Supplemental Figure 1

660 **Figure S1. *kcnh2a* is required for fin overgrowth in regenerating *lof*^{t2} animals.**

(A–C) Representative images of regenerated caudal fins at 27 days post-amputation (dpa) from (A) wildtype control, (B) *lof*$^{t2/t2}$*; kcnh2a*$^{+/+}$, and (C) *lof*$^{t2/t2}$*; kcnh2a*$^{b1391/b1391}$ fish. The dashed yellow line indicates the site of fin resection and scale bars represent 1 mm. **(D)** Quantification of fin ray outgrowth of wildtype (blue squares), *lof*$^{t2/t2}$*; kcnh2*$^{+/+}$ (red triangles), and *lof*$^{t2/t2}$*;*

665 *kcnh2a*$^{b1391/b1391}$ (green circles) fish at 27 dpa. Each data point represents the normalized length of ray 3 from an individual animal of the indicated genotype.

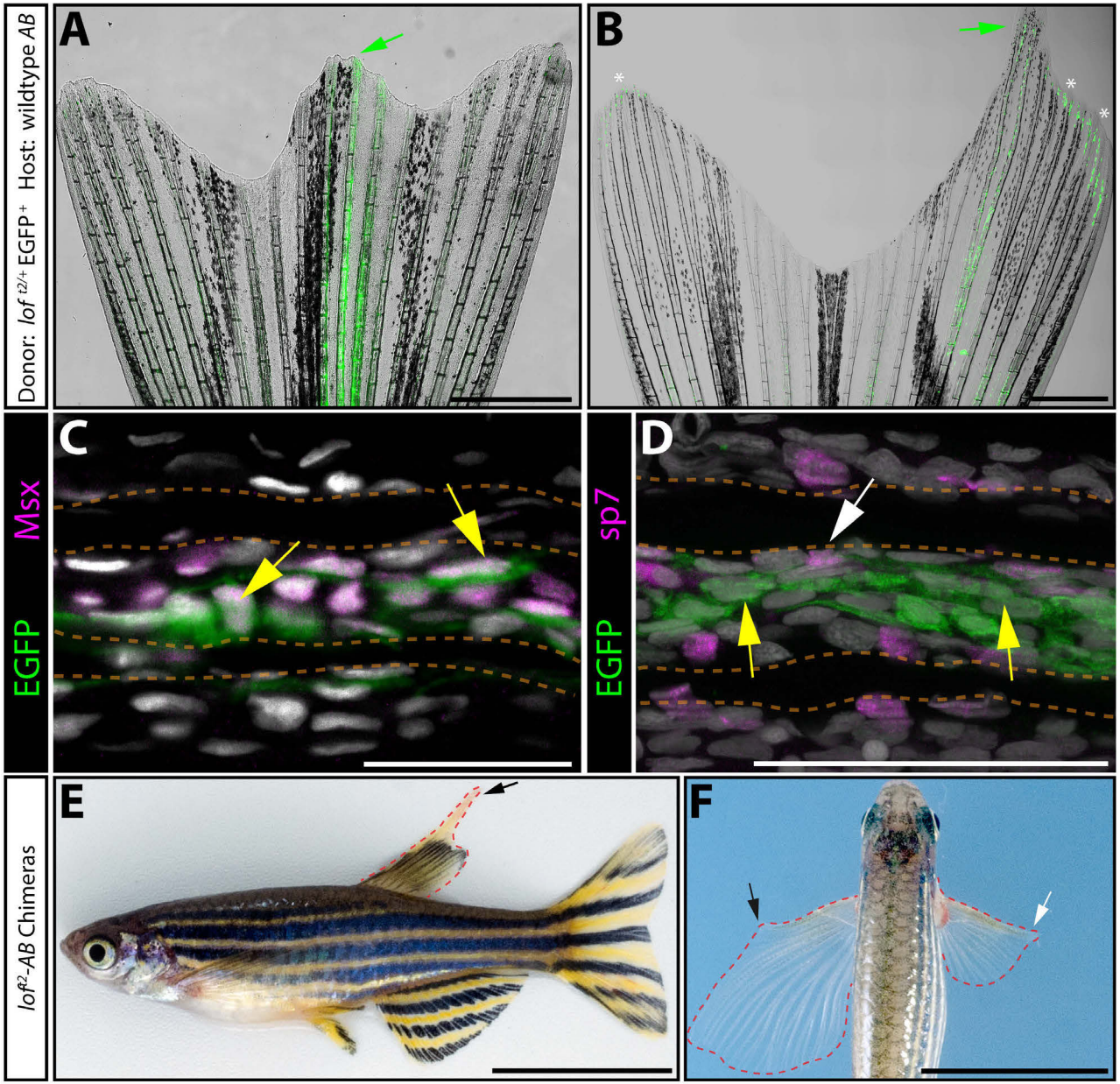

Supplemental Figure 2

Figure S2. *lof^{t2}-AB* chimeras reinforce *lof^{t2}*-ectopic *kcnh2a* acts within the intra-ray
670 **mesenchyme lineage.**

(A, B) Superimposed epifluorescence/DIC images showing two additional examples of overgrown caudal fin rays from chimeric animals generated by transplanting blastula stage EGFP^{+} *lof$^{t2/+}$* cells into wildtype *AB* embryos. Green arrows indicate overgrown rays containing EGFP^{+} cells derived from *lof$^{t2/+}$* embryos and white asterisks point to auto-fluorescent pigment
675 cells. Scale bars indicate 1 mm. **(C, D)** Immunostaining using EGFP and (C) Msx or (D) sp7 antibodies on sections from overgrown chimeric caudal fins generated by blastula-stage transplantation (upper panel). In (C), yellow arrows indicate EGFP^{+}/Msx^{+} intra-ray mesenchymal cells derived from *lof$^{t2/+}$* transplants. In (D), the yellow arrows indicates the EGFP^{+} mesenchyme, the white arrow points to a sp7^{+} osteoblast. Dashed orange lines outline fin
680 ray bones. Scale bars represent 50 μm. **(E)** Lateral whole animal view of a distinctive *lof^{t2}-AB* chimera. The black arrow indicates overgrown dorsal fin tissue. The scale bar represents 1 cm. **(F)** Dorsal view of a *lof^{t2}-AB* chimera to highlight contralaterally distinct pectoral fin sizes. Dashed red lines outline the pectoral fins. The black and white arrows points to overgrown and normal sized fins, respectively. The scale bar represents 1 cm.

685

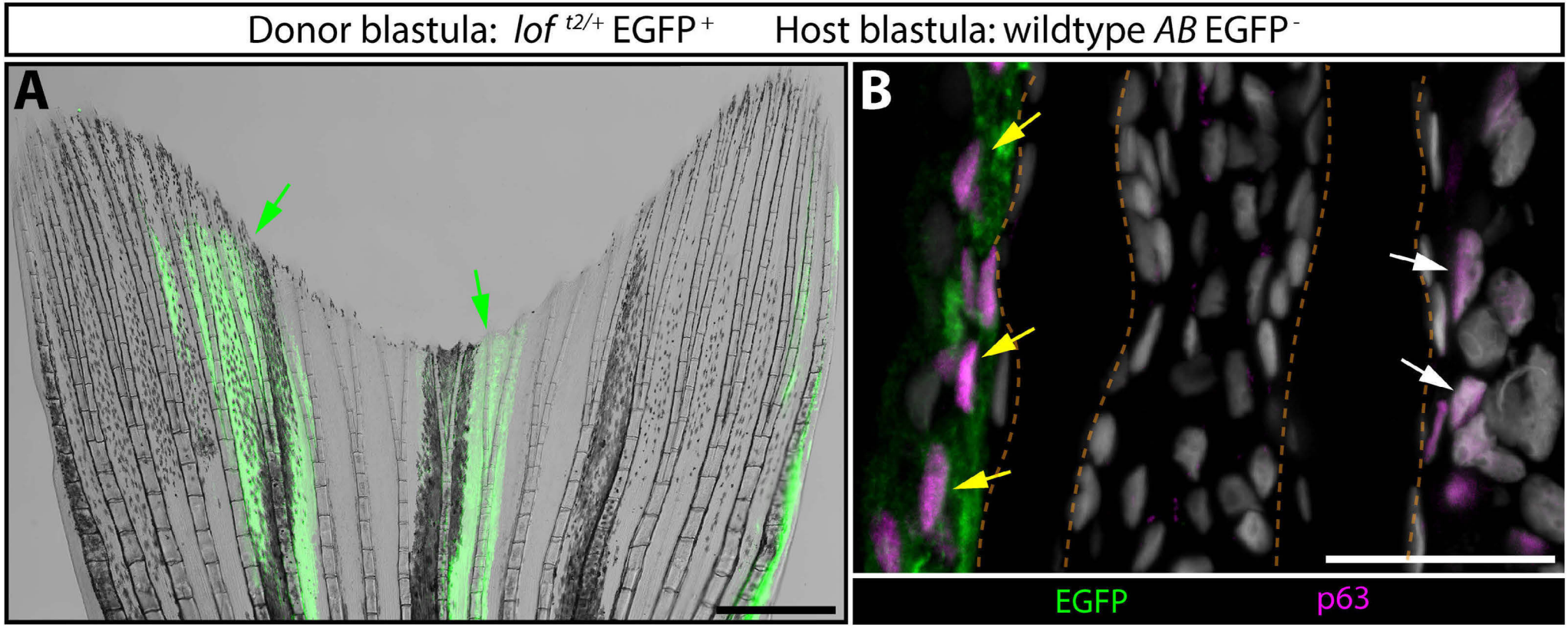

Supplemental Figure 3

Figure S3. Epidermal *lof*^{t2}-AB chimeric caudal fins do not overgrow.

(A) A DIC/fluorescence-imaged caudal fin from a *lof*^{t2}*-AB* chimera with EGFP^{+} epidermis (green
690 arrows). The scale bar represents 1 mm. **(B)** Immunostaining of sections from the same fin using EGFP and p63 antibodies to detect transplanted *lof*$^{t2/+}$ cells (green cells) and epidermal cells (magenta nuclei), respectively. Yellow arrows point to chimeric EGFP^{+}/p63^{+} epidermal cells and white arrows indicate p63^{+} host-derived epidermis. Nuclei are Hoechst-stained (gray), dashed orange lines outline fin rays, and the scale bar shows 50 μm.

695

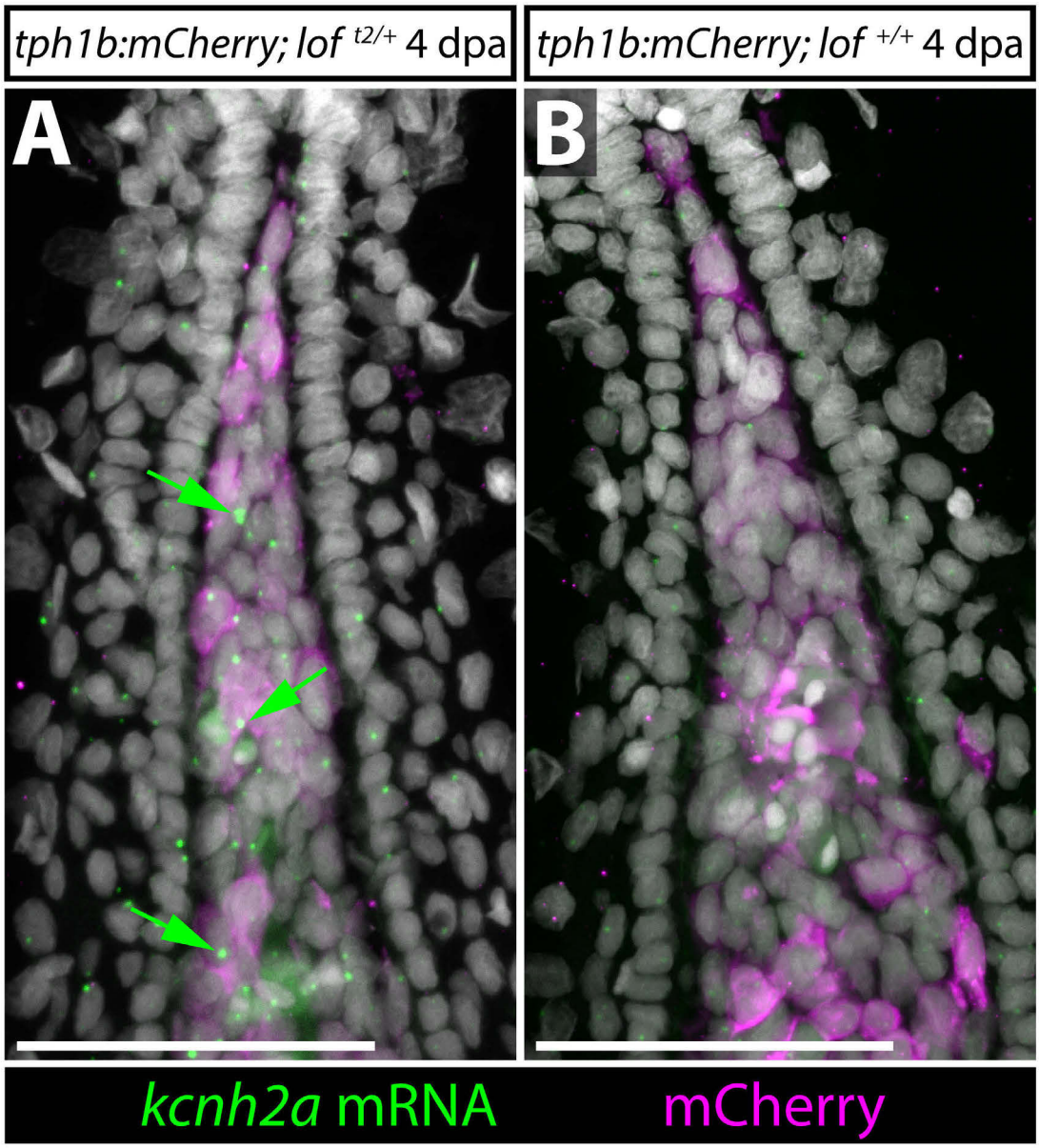

Supplemental Figure 4

Figure S4. *kcnh2a* is expressed in *tph1b:mCherry*-positive distal niche cells of *lof*^{t2} regenerating caudal fins.

700 **(A, B)** Confocal maximum intensity projection images showing combined *kcnh2a* RNAscope and mCherry antibody staining on 4 dpa fin sections from (A) *tph1b:mCherry; lof*$^{t2/+}$ and clutchmate (B) *tph1b:mCherry; lof*$^{+/+}$ animals. Green arrows point to distal *tph1b:mCherry; lof*$^{t2/+}$ niche cells expressing *kcnh2a* mRNA. Hoechst-stained nuclei are in gray. The scale bars represent 50 μm.

705

Table S1. RNA-Seq table showing differentially expressed transcripts in *lof*^{t2} vs. wildtype fins at 4 dpa.